Appl. Phys. B (2015) 118:219–229
DOI 10.1007/s00340-014-5973-0

Applied Physics B
Lasers and Optics

Polymeric fiber sensor for sensitive detection of carbon dioxide based on apodized wavelength modulation spectroscopy

Mehran Mohammadi Jozdani · Alireza Khorsandi · Saeed Ghavami Sabouri

Received: 25 June 2014 / Accepted: 6 December 2014 / Published online: 18 December 2014

Abstract The performance of an optical sensor that employs an unbuffered polydimethylsiloxane (PDMS)-cladding fiber optic is demonstrated for the sensitive detection of CO_2 gas in the near-infrared region for around 1.57 μm using the apodized 2f/1f wavelength modulation spectroscopy method. The permeability and diffusion characteristics of the PDMS fiber have been theoretically examined and numerically simulated. The results of the simulation are verified by an experimental setup containing a DFB laser source and 5-m-coiled unbuffered PDMS fiber placed in a pre-vacuumed cell filled with about 980 ± 10 Torr of pure CO_2 gas. A minimum detectable absorption of ~0.9×10^{-4} is measured, corresponding to a detection sensitivity of ~4.5×10^{-11} $cm^{-1}/Hz^{1/2}$. The effect of the scaling *k*-factor on the apodized signal is subsequently studied, showing close agreement between the simulation and experimental results.

1 Introduction

Evanescent wave (EV) absorption spectroscopy has been recently developed and widely implemented as an effective method for characterization of a variety of both physical and chemical variables in research, industry and medicine. This method has some benefits such as nondestructivity, online response and safety in detection. It is based on the penetration of a fraction of the guided light into the lower index region of an optical fiber and its radial exponential decay while propagating along the fiber length. This has turned it into an exceptional candidate for the design and fabrication of a variety of fiber-based sensors. Moreover, different experimental designs and theoretical investigations have been brought about by discussing the increase of the sensitivity and dynamic range of such sensors. In 1994, Gupta et al. [1] published a paper basically describing the effects of launching conditions and geometry of the sensing region on the sensitivity of the EV fiber optic sensor. A comprehensive three-dimensional model has also been formulated by Messica et al. [2] to investigate the performance of an EV-based step-index multimode optical fiber sensor. It is shown that the penetration depth of the EV wave is one of the key parameters playing an important role in developing high sensitivity sensors crucial to the tracing of weak signals in the limits of ppb and ppt levels of concentrations. Since the penetration depth is inversely proportional to the refractive index of a medium surrounding the fiber core, EV-based absorption spectroscopy around an uncladded core has introduced a very attractive and promising field of research. One example is the in situ monitoring of silver thin film deposition rate using a 0.01 m uncladded region of a multimode fiber as sensing element, while the target was irradiated by a Q-switched Nd:YAG laser [3]. Another example is the trace analysis of Fe^{+3} in water using a 12 cm uncladded portion of a plastic-clad silica fiber at the detection limit of ~1 ppb [4]. In many alternative cases, the uncladded fiber is uncritically bent to increase the number of reflections at the interface. In this context, a fiber optic EV sensor is employed by Orghici et al. [5] to determine the TNT and CO_2 concentrations dissolved in water. The sensor consisted of a 4-m-long uncladded multimode fiber coiled and fixed on a 5-cm-diameter and 16-cm-long Teflon mount. In recent years, such sensor geometry has been developed for the detection of liquids, gases and thin layers replacing the fiber cladding by the examined sample. In an

M. M. Jozdani · A. Khorsandi (✉) · S. G. Sabouri
Department of Physics, University of Isfahan,
81746-73441 Isfahan, I. R. Iran
e-mail: a.khorsandi@phys.ui.ac.ir

instructive experimental work, the performances of a fabricated EV sensor is demonstrated by Shojaei et al. [6] for pH measurement of methyl red solution in a relatively wide range using a 1-m-coiled uncladded optical fiber as sensing element. It is also demonstrated that the detection sensitivity can be simultaneously enhanced by using tapered fiber for the sensor head. By tapering a fiber, the number of internal reflections is significantly enhanced, and a large sensing area along a small diameter can be achieved, while the penetration depth is increased. A comparative study is conducted to characterize the performance of a very flexible and in situ refractive index sensor employed for epoxy resin monitoring in a wide range of the spectrum from 1,450 to 2,250 nm [7]. At the same time, the theoretical and experimental implications of a bi-tapered multimode optical fiber is made by Grazia et al. [8] to improve the efficiency of the measurement through modification of the core geometry. By using a scanning near field optical microscope, the EV field distribution around the tapered region of an optical fiber is measured and numerically modeled to introduce a comprehensive reference for the optimization and fabrication of various types of tapered fibers [9]. A novel diagnostic technique is proposed by Li et al. [10] based on the EV absorption spectroscopy of thin organic film deposition in gas discharge plasmas using a sensor head fabricated from a tapered infrared fiber. Soon after a U-shaped tapered fiber sensor is also employed by Kraft et al. [11] to develop the performance of the utilized sensor geometry for measuring volatile hydrophobic organic compounds in the marine environment. The dependence of the EV penetration depth on the operating wavelength of the incident light and the refractive index of the medium surrounding the core of a tapered optical fiber is theoretically analyzed and numerically simulated by Lu et al. [12]. Particularly, the most applications of the EV fiber sensors are in water analysis within the near-(NIR) and mid-infrared (MIR) where the EV penetration depth is directly proportional to the operating wavelength. For instance, the solid–liquid phase transition of water and heavy water around 4 μm were investigated [13]. The EV-based fiber sensor application is to detect and identify the cancer cells [14], and recently, it has been used in medical diagnosis of blood compounds such as glucose in vitro [15]. The former application benefits from the FTIR technique to identify spectral properties of intact cells. A modern application of an optical fiber with tapered structure is demonstrated by De-Jun et al. [16] for the refractive index measurement of a plastics fiber, indicating the enhancement of sensor linearity for a smaller tapered region. Due to the advanced modern technology, different design and structures of these fiber sensors have been made and developed to enhance the sensitivity and selectivity. In this regard, a tunable fiber ring laser sensor has been fabricated for gas sensing using photonic crystal fiber [17]. The laser light is injected into the fiber cladding by a long periodical grating, and the air holes of the fiber core act as an absorption cell for sensitive and selective measurement of ammonia concentration. The sensor indicates minimum susceptibility to the temperature and humidity changes. A new photonic crystal fiber sensor is numerically simulated for detection of methadone in water by Mescia et al. [18] to optimize the sensor performance and refinement. It is accomplished through varying of the fiber characteristics such as the thickness of polymeric layer, the hole diameter and the hole distribution on the fiber cross section with the emphasis on the enhancement of the EV field interaction with the polymeric layer. This led to the suggestion of a suitable fiber cross section. It has also been shown by Luo et al. [19] that a silver nanoparticle-modified EV optical fiber sensor is also capable of reaching a higher sensitivity required for the concentration changes of methylene. An intensive study on the progress of optical fiber sensors with the emphasis on fiber Bragg grating, long period grating and hollow core fibers has been carried out by Mescia and Prudenzano [20]. Similarly, several experimental arrangements based on the EV absorption spectroscopy have been realized for the monitoring of a variety of molecular species like CO_2 [5] and hydrocarbons [21, 22] which are particularly considered as a global challenge in climate change and energy resources. However, the main drawback faced by these configurations is the susceptibility of the sensor head to the bending radius, temperature tensions and environmental disturbances, resulting in the breaking of the uncladded and tapered fiber and making it very fragile. Furthermore, regarding sticky and corrosive samples, the sensor must be alternatively recovered and cleaned by using chemical solutions which in turn affects and reduces the sensor lifetime and durability. This makes the sensor vulnerable to outdoor applications such as sensing in harsh environments. The use of sensitive cladding materials can be considered as an alternative solution to the above sensor structures. This allows the sample to diffuse into the cladding region and to interact with the penetrated EV field at the interface.

The diffusion of analyte into the silicone clad of an optical fiber chemical sensor was analytically studied by Blair et al. [23] to obtain the transport rates of polar analytes. The study led to the developing of a single-parameter model to calculate the diffusion coefficients of several hydrocarbon compounds. The obtained results have been verified by setting up an experimental apparatus and measuring the calculated parameters in a dimethylsiloxane material.

It is demonstrated that the diffusion characteristics of analytes may be influenced by the sensor condition. On the other hand, the sample's penetration into the fiber cladding is simultaneously determined by diffusion, permeability and solubility coefficients of the cladding material, while the influence

of pressure and concentration of sample surrounding the fiber are crucial. Since different samples have different penetration coefficients, the application of this method is quite advantageous for the diagnosing of overlapped absorption lines. In this method, the sample is penetrated into the permeable cladding made of a specific polymer known as polydimethylsiloxane (PDMS) which has very desirable physical characteristics [24, 25] for penetrating a wide range of materials in liquid and gas phases. An example demonstrated by D'Orazio et al. [26] is a realistic design of three different planar waveguides covered by 400 nm thickness of PDMS layers. The optimum performance of the sensor is obtained with a 2.6-cm-long waveguide at a wavelength of 260.64 nm for 200 ppm of toluene concentration measurement dissolved in water. The simulation results confirm that for guided and leaky TE and TM modes, the absorbance feature of the sensor is different. The design of an optical sensor array for hydrocarbon monitoring is accordingly reported by the same research group [27] to obtain a suitable waveguide cross section and geometry. The sensor array consisted of four hollow waveguides wrapped by equal thickness of PDMS polymeric layers for simultaneous measurement of four hydrocarbons dissolved in water. Quite recently, an interferometric chemical sensor is reported by St-Gelais et al. [28] in which the sensing procedure was based on the shifts of the Fabry–Perot interferometer resonance wavelengths that are induced by the swelling and refractive index variation of the utilized polymers upon absorbing m-xylene and cyclohexane analytes at the detection limits of 1.6 and 6.3 ppm, respectively.

In the present work, a silicon-core PDMS cladding optical fiber is used as sensing element for trace measurement of CO_2 molecules inside a pre-vacuumed laboratory cell. It is experimentally performed by leaving the coiled fiber into a cell containing 980 ± 10 Torr of pure (~99.99 %) CO_2 gas. The output beam of a commercial NIR–DFB laser is launched into the utilized fiber and scanned over the absorption lines of the CO_2 molecule around 1.57 μm. By penetrating the CO_2 species into the permeable polymer cladding of the utilized PDMS fiber and interacting with the sustained EV field, it is then detected at the output end of the fiber using a sensitive detection scheme. To improve the signal-to-noise ratio (SNR) of the experiment, laser current is modulated at a certain frequency to establish a sensitive detection based on wavelength modulation spectroscopy (WMS). The limitations on the signal resolution is avoided through using the apodized WMS-2f/1f [29] along with a lock-in amplifier. Simulation of the results has also been performed using the real practical data associated with the experimental arrangement provided in our laboratory. The results have shown that the fabricated optical sensor shows promise for sensitive and selective spectroscopy of CO_2 species, and good consistency is obtained between the experiment and simulation.

2 Theory of operation and simulation results

Based on mutual and independent penetrating of either sample from the surrounding environment or EV field from the fiber core into the cladding region, field–matter interaction can be established, while the transmitted light collects the required information about the physical and chemical characteristics of the sample. Basically, it is based on the exponential decreasing of transmitting power as

$$P(z) = P_0 \exp(-\xi z) \tag{1}$$

due to an absorbing medium surrounding the fiber. Here, P_0 is the input power at $z = 0$, and ξ is the EV absorption coefficient of the sample.

For a multimode step-index fiber of core radius a which cladding has been replaced by a lossy medium of refractive index $\tilde{n}_2 = n_2 + i\kappa$, we have [30]

$$\xi = NT \tag{2}$$

where N is the number of reflections per unit length, and T is the Fresnel transmission coefficient at the interface. The former can be increased by either increasing the length or bending of the fiber sensor and [30, 31]

$$T = \frac{\alpha \lambda n_2}{\pi (n_1^2 - n_2^2)} \frac{\cos\theta}{\sqrt{\sin^2\theta - \sin^2\theta_c}} \tag{3}$$

where λ is the wavelength of incident light in vacuum, $\alpha = 4\pi\kappa/\lambda$ is the wavelength-dependent bulk absorption coefficient of the absorbing medium, θ and θ_c are, respectively, the incident and critical angles at the interface and n_1 is the refractive index of the core. Because in such cases, $n_1 > n_2$, the weakly guiding approximation is no longer valid, making θ_c very small. Therefore, the modes with $\theta > \theta_c$ are allowed to be guided by the fiber at a wide range of angles greater than θ_c. This results in the contribution of many modes in the EV area, and hence, a stronger field–matter interaction can be formed. At the same time, the number and the order of modes are accordingly determined by the normalized frequency parameter V and the satisfied boundary conditions at the interface, implying that for higher values of V, the EV field is stronger.

In our case, where a fiber cladding is made of a permeable and lossy PDMS material, the weakly guiding approximation holds because$n_1 \approx n_2$, making θ_c larger and V smaller than those considered in the previous case. This led to the contribution of only selected modes in the EV region with a range of incident angles lesser than that of uncladded fiber. Here, the Fresnel transmission coefficient changes to [31, 32]

$$T = \frac{\alpha \lambda}{\pi \theta_c'^2 n_2} \frac{\theta_z}{\sqrt{\theta_c'^2 - \theta_z^2}} \tag{4}$$

with $\theta_c' \simeq \sqrt{1 - \left(n_2/n_1\right)^2}$ and $\theta_z = \pi/2 - \theta$.

In either case, the bending causes the light beam to hit the interface at smaller angles of θ which closely approaches θ_c. Therefore, a large number of reflections can be accumulated in the bent region, and according to Eqs. (3) and (4), the T coefficient increases. This in turn resulted in the much stronger interaction of the EV field with the surrounding environment due to the increase of the NT factor. On the other hand, the sensitivity of the bent fiber sensor is dependent on the bending radius which for a multimode fiber is limited by the critical value given by [33]

$$R_c = \frac{3}{4\pi}\frac{n_1^2\lambda}{\left(n_1^2 - n_2^2\right)^{3/2}}. \tag{5}$$

Moreover, it is found by calculations that the formulation of the EV absorption coefficient is different for meridional and leaky skew rays [34], consequently having different contributions to the absorption of EV wave. The results of this investigation indicate that compared to the meridional rays, the skew rays have much smaller participation in EV wave absorption. In general, for a fiber with cylindrical symmetry, the EV wave outside the core is described by the modified Bessel function, and at a relatively large radial distances of r from the fiber axis, the associated electric field can be approximated by [33]

$$E_{\text{clad}} = E_0\frac{e^{-\left|k_r^{\text{clad}}\right|r}}{\sqrt{\left|k_r^{\text{clad}}\right|r}} \tag{6}$$

where E_0 is the electric field at the core–cladding interface, and k_r^{clad} is the radial wavenumber. Consequently, the EV penetration depth in the cladding region can be formulated as

$$d_p = \frac{1}{\left|k_r^{\text{clad}}\right|}, \tag{7}$$

indicating an order of the incident wavelength. Under the plane-wave approximation and examining the meridional rays, it can be recalculated to obtain [35]

$$d_p = \frac{\lambda}{2\pi\sqrt{n_1^2\sin^2\theta - n_2^2}}. \tag{8}$$

Once the optical fiber is characterized, the penetration of the absorbing sample in the cladding region can be considered as a secondary control factor to optimize the mechanism of EV field decay and to increase the performance of the sensing procedure as well. This can be achieved by a special type of optical fibers employing from a permeable cladding material mostly fabricated from polymer compounds. This allows the core–cladding interface to be experienced by the particles of the surrounding sample.

In order to study the variables affecting the sample penetration into a permeable polymer cover, we follow the second Fick's law where the time and spatial variations of the concentration of the penetrating sample, $C(r,t)$, are related to the following time-dependent diffusion equation by assuming cylindrical symmetry for the utilized fiber [36]

$$\frac{\partial C(r,t)}{\partial t} = \frac{D}{r}\frac{\partial}{\partial r}\left[r\frac{\partial C(r,t)}{\partial r}\right] \tag{9}$$

where $D\,[\frac{\text{cm}^2}{\text{s}}]$ is the diffusion coefficient, and r[cm] is the radial coordinate along the propagation direction. Assuming $C(r,t) = c(t)\,\text{g}(r)$, the time variation of the diffused concentration can be obtained by solving Eq. (4) through variables separation to find

$$c(t) = c_e\left[1 - \exp(-\gamma Dt)\right] \tag{10}$$

where c_e is the sample concentration at the equilibrium time, and γ is the separation constant that relates to the solutions of the Bessel function. Among the available materials which are recently being used for fiber cladding fabrication, polymers have shown excelling optical characteristics and sufficient permeability. Based on Eq. (10), the variation of the diffused concentration with time is simulated in Fig. 1 for different types of polymers commonly used by manufacturers for cladding structure.

The characteristics of the polymers used for the simulation have been summarized in Table 1.

As it can be seen from the results shown in Fig. 1, PDMS and PPMS polymers show a very appreciable permeability feature with very rapid response such that after about 60 min, $c(t)$ reaches the equilibrium value, c_e. This led to the establishment of an adequate interaction with the penetrated sample in the EV area very close to the core–cladding interfaces of those polymer-based optical fiber sensors. Therefore, because of flexibility and availability, our work is accomplished with the PDMS cladding optical fiber. To further identify the sensing performances and permeability

Table 1 Characteristics of the polymers used in plotting Fig. 1 [37]

Polymer type	Diffusion coefficient, $D\,[\frac{\text{cm}^2}{\text{s}} \times 10^6]$ for CO_2 gas	Solubility parameter $\delta\left(\text{J}/\text{cm}^3\right)^{0.5}$
PDMS: poly(dimethylsiloxane)	11	14.5
PTFPMS: poly((trifluoropropyl)methylsiloxane)	3.2	17.1
PPhMS: poly(phenylmethylsiloxane)	0.8	18.8
PPMS: poly(propylmethylsiloxane)	12	14.8

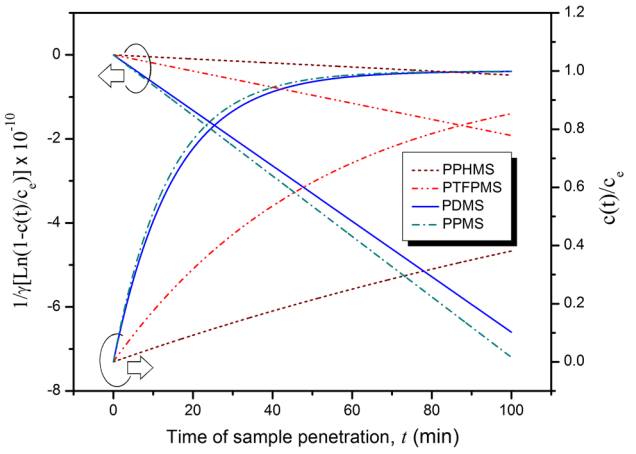

Fig. 1 Diffusion of carbon dioxide (CO_2) into the cladding of an optical fiber simulated for four different types of polymers as commonly utilized for fabricating the fiber cladding. It is also assumed that $\gamma = 10^{-4}$

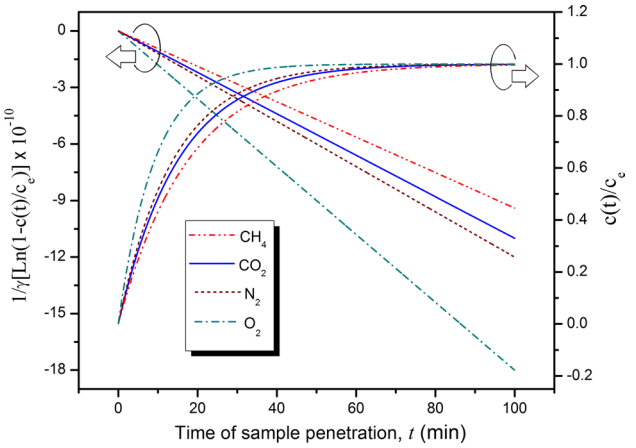

Fig. 2 Permeability characteristics of PDMS polymer versus time for different gas samples. Simulation is performed at standard temperature and pressure (STP) conditions. The γ coefficient is the same as used in Fig. 1

characteristics of the PDMS material, the penetration behavior of different gas samples into the utilized polymer is calculated and simulated in Fig. 2 at room temperature and standard pressure.

It is evident from the above plot that the PDMS polymer has sufficient and relatively fast response to the CO_2 gas sample where $c(t)$ is gradually relaxed to the equilibrium. As a result, a PDMS-based optical fiber looks promising for sensing external environment factors when benefiting from an adequate laser source. Therefore, a combination of a PDMS fiber sensor and absorption spectroscopy is capable of making a very selective and sensitive tracing of atomic and molecular species in either gas or liquid phases. The latter is described by the well-known Beer–Lambert law given by

$$I(\nu) = I_0(\nu)\exp[-\alpha(\nu)] = I_0(\nu)\exp[-S_{nm}\phi(\nu-\nu_0)P_tN_xL] \quad (11)$$

where $I(\nu)$ and $I_0(\nu)$ are, respectively, the input and output intensities, $S_{nm}(\mathrm{cm}^{-2}/\mathrm{atm}^1)$ is the absorption line strength of transition $n \rightarrow m$,$\phi(\nu-\nu_0)$ is the Voigt lineshape function, P(atm) is the total pressure, N_x is the mole fraction of gas sample and L(cm) is the absorption path length. In order to increase the sensitivity of detection, we used the wavelength modulation spectroscopy (WMS) technique in which the injection current of the utilized laser source is sinusoidally modulated over a few tens of kHz. This in turn resulted in the modulation of the sample transmittance and therefore in higher harmonics and particularly first and second harmonic components of the modulated reference signal as

$$\begin{aligned} X_{1f} &= \frac{G\bar{I}_0}{2}\left[H_1 + i_1\left(H_0 + \frac{H_2}{2}\right)\cos\psi_1 + \frac{i_2}{2}(H_1+H_3)\cos\psi_2\right] \\ X_{2f} &= \frac{G\bar{I}_0}{2}\left[H_2 + \frac{i_1}{2}(H_1+H_3)\cos\psi_1 + i_2\left(H_0 + \frac{H_4}{2}\right)\cos\psi_2\right] \end{aligned} \quad (12)$$

where G is the electro-optical gain, $\bar{I}_0$ is the average laser intensity over modulation period, H_i are symmetrical and anti-symmetrical components of the modulated signal, ψ_1 and ψ_2 are, respectively, linear and nonlinear relative phase shifts between laser intensity and reference sinusoidal frequency and i_1 and i_2 are the linear and nonlinear modulation coefficients related to the intensity modulation of the laser beam, respectively. The X_{1f} and X_{2f} signals can be detected after filtering out of undesirable noises through making use of a lock-in amplifier. The key advantage of using the WMS technique is the possibility of using the 1f signal as a baseline crucial to the field environments where quantitative measurement is rigorously correlated with the nonabsorbing base line that is inaccessible. Accordingly, a calibration-free WMS method is proposed by normalizing of the 2f signal by the 1f signal, but it is utilizable just at the thin optical limit where $e^{-\alpha(\nu)} \simeq 1-\alpha(\nu)$. Subsequently, by using the WMS-2f/1f technique, the experimental configuration held against optical and electrical perturbations, including vibration and misalignment of the optical setup and undesirable intensity fluctuations occurring in the laser beam intensity, and therefore repetitive on-site calibration is avoided. However, for the absorbances exceeding the optically thin limit, the negative branch of the WMS-1f signal tends to zero. This behavior is simulated in Fig. 3 for the R(32) CO_2 absorption line centered at 6,369.408 cm^{-1} with a line strength of 7.55×10^{-24} $\mathrm{cm}^{-1}/(\mathrm{mol/cm}^2)$, while its absorbance is changed from 0.01 to 0.04. In order to verify the simulation results, we used the experimental conditions associated with the setup arranged in

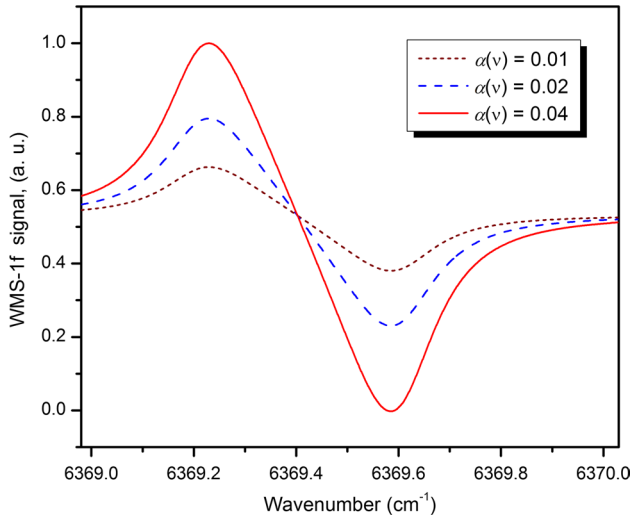

Fig. 3 Simulated WMS-1f signal for different absorbances, $\alpha(\nu)$, starting from 0.01 as the optically thin limit, toward the thick limit specified by 0.04 for the R(32) CO_2 absorption line at 6,396.408 cm^{-1}. For the simulation, we assumed that the modulation frequency and index are 3 kHz and 2.2, respectively

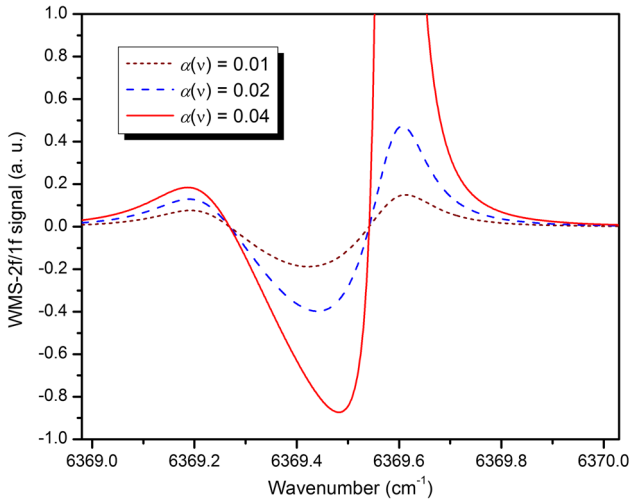

Fig. 4 Simulated WMS-2f/1f for a range of CO_2 absorbances while reaching the optically thick limit at $\alpha(\nu) = 0.04$. The same characteristics as used in Fig. 3 are employed in this figure too

our laboratory and the CO_2 line characteristics provided by the Hitran database [38]. Therefore, our simulation was performed for room temperature and 980 Torr of gas pressure as required for obtaining maximum penetration of CO_2 gas into the PDMS cladding of the fiber sensor. Under the above pressure condition, the Doppler broadening is assumed quite negligible, and the lineshape function of the specified line is described by the gas pressure that can be approximated by the Lorentzian linewidth, $\Delta\nu_L$. Thus, according to the self-broadening coefficient of the R(32) CO_2 line inferred from the Hitran database [38], we calculated $\Delta\nu_L \simeq 0.089$ cm^{-1}.

The plot confirms that as the CO_2 absorbance exceeds the thin limit, the descending branch of X_{1f} reaches zero, resulting in a trend to infinity in the WMS-2f/1f signal which causes troubling uncertainty in the measurement and hence makes the method inefficient for environmental researches. Figure 4 illustrates how, beyond a certain limit of CO_2 absorbance, uncertainties can be effectively developed to influence the quantitative results.

The tendency of the WMS-2f/1f signal to infinity along with the displacement of the absorption peaks toward longer wavenumbers at higher absorbances is clearly observed from Fig. 4. To gain further development in the WMS-2f/1f technique and to overcome the experienced disadvantages, a heuristic approach known as apodized WMS-2f/1f method is mathematically suggested where X_{1f} is modified to X_{1f}^{apodized} as

where k is the scaling factor which acts as control parameter on the signal fluctuations and provides maximum resolution for the WMS-2f/1f signal with minimum peak displacement and without altering the intrinsic characteristics of the absorption line. Figure 5 simulates the effect of the apodizing procedure and the k factor on the WMS-2f/1f signal for the R(32) CO_2 absorption line under similar conditions as considered in Fig. 3. In order to indicate the performance of the demonstrated apodized method, the results have been depicted for $\alpha(\nu) = 0.04$ which was causing the infinity. Based on the R(32) line characteristics, its Lorentzian linewidth is then calculated $\Delta\nu_L \simeq 0.088$ cm^{-1} with a negligible Doppler width.

As it can be observed, the apodized method and the effect of the scaling k factor on the signal resolution are very significant. No remarkable peak displacement can be detected from the plot, while the WMS-2f/1f signal is narrowing with the increase of the k value. Moreover, it can be applied for either thin or thick optical limits. This provides an important advantage over the distinction of two or more neighboring absorption lines covered by the scanning range of an appropriate laser source. Whenever it is coupled with an appropriate laser source tunable within a certain range of CO_2 absorption lines, it is possible to increase the sensitivity of detection using the characterized PDMS optical fiber. According to the DFB laser source specifications and its inherent tuning range utilized in the oncoming experimental part of this work, two absorption lines of

$$X_{1f}^{\text{apodized}} \simeq \frac{G\bar{I}_0}{2}\left\{ i_1 \cos\psi_1 + k\left| H_1 + i_1\left(H_0 + \frac{H_2}{2} - 1\right)\cos\psi_1 + \frac{i_2}{2}(H_1 + H_3)\cos\psi_2 \right| \right\} \tag{13}$$

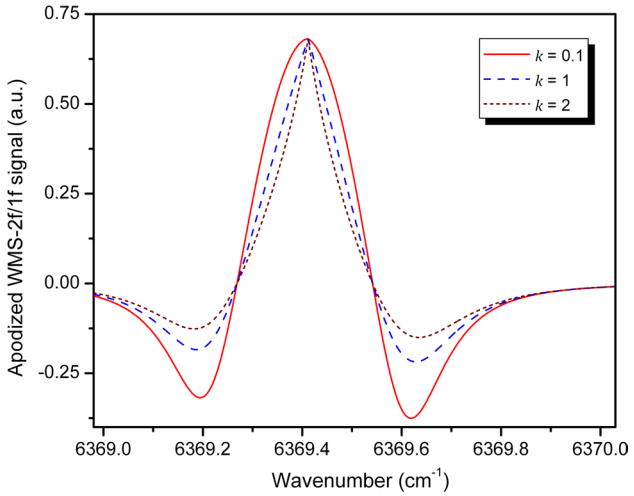

Fig. 5 Apodized WMS-1f/2f signal simulated for the R(32) CO_2 absorption line, while the scaling factor is varied for $k = 0.1$, 1 and 2, respectively. The CO_2 absorbance is assumed $\alpha(\nu) = 0.04$, and other parameters are similar to those of Fig. 3

CO_2 molecules identified by R(32) and R(34) have been selected and simulated in Fig. 6, at room temperature and gas pressure of 980 Torr.

Apparently, by increasing the scaling k factor up to 2, the width of the WMS-2f/1f signals is decreased by about two orders of magnitude. Therefore, the significance of the utilized technique over the optically thin region is clearly demonstrated without any singularity or peak displacement while the shape of the signal is preserved.

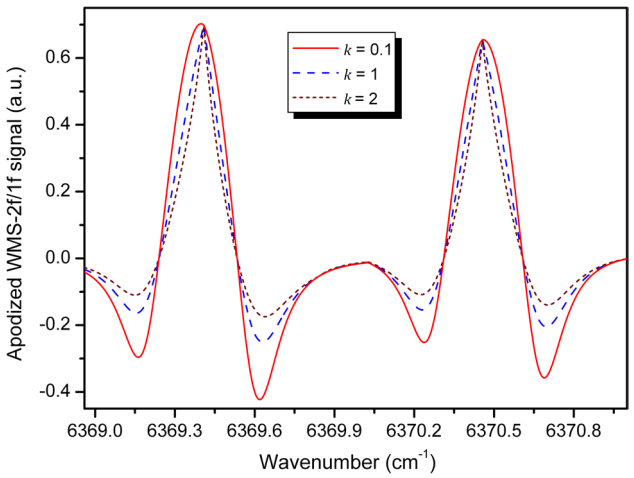

Fig. 6 Simulated apodized WMS-2f/1f signal for R(32) and R(34) absorption lines of the CO_2 molecule centered at 6,396.408 and 6,370.457 cm^{-1} with line strength of 7.55×10^{-24} and 6.19×10^{-24} $cm^{-1}/(mol/cm^2)$, respectively. Modulation frequency and index are, respectively, assumed 3 kHz and 2.2. The simulation is performed for the CO_2 absorbance of $\alpha(\nu) = 0.04$ for different k factor values

3 Experimental setup and results

In Fig. 7, the experimental arrangement is schematically indicated.

The output beam of a DFB laser (Laser components Ltd.) is used as light source. It provided a maximum output power of 5 mW at center wavelength of 1.57 μm with a temperature and current tuning capabilities of 0.1 nm/K and 3.5 GHz/mA, respectively, within a certain range of ro-vibrational transition lines of CO_2 molecule. By applying a combination of ramp voltage and a flexible sine wave superimposed on the injection current, simultaneous scanning and modulating of the laser wavelength over a desirable range was possible. The evanescent field sensor consisted of a commercially available PDMS silica core fiber (fiberguide ind.) with a core and cladding diameters of 100 and 200 μm, respectively, and a nylon buffer with a thickness of 35 μm. In order to fabricate a truly sensing element, the outer buffer was chemically removed over about 5 m of its length. This was performed by boiling the fiber in a propylene glycol solution heated to ~180 ± 1 °C during 30 s. The provided PDMS fiber was then coiled and fixed on a metallic mount which had a height and diameter of about 5 and 15 cm, respectively. This enabled increasing the EV field at the bent core–cladding interfaces and protecting the fabricated fiber against breakage and undesirable stresses. Two objective lenses with a focal length of 1 mm were used to couple the DFB laser beam with the fabricated sensor and to image the transmitted light on the 1 mm^2 active area of a detector. The latter was a high speed InGaAs photodiode (Thorlabs, FGA20) as detector with a spectral response from 1,200 to 2,600 nm and a fast rise/fall time of 23 ns. A commercial data acquisition card (DAQ, NI 6036) along with a PID controller algorithm provided in the LabVIEW environment were implemented to modulate the laser injection current up to 3 kHz at optimum modulation index of 2.2 as utilized for the simulation. Further feasibility of using the above configuration is the simultaneous recording of the WMS-1f and 2f signals with about 200 kS/s of sampling rate. This enabled the generation of the apodized WMS2f/1f signal nearly at the same sampling rate. The required frequency scanning of the DFB laser around the R(32) and R(34) absorption lines of the CO_2 molecule was accomplished by using a 10 s sawtooth ramp superimposed on the injection current of the laser.

As shown in Fig. 7, the coiled sensor was then placed in a pre-vacuumed stainless steel cell and filled with 980 ± 10 Torr of pure CO_2 gas (99.99 %). This corresponds to a CO_2 absorbance of about 0.035, quite within the range governed by the optically thick limit.

To ensure that gas is sufficiently penetrated into the PDMS cladding and reaching the equilibrium condition, the sensor is left inside the cell for an adequate time, and

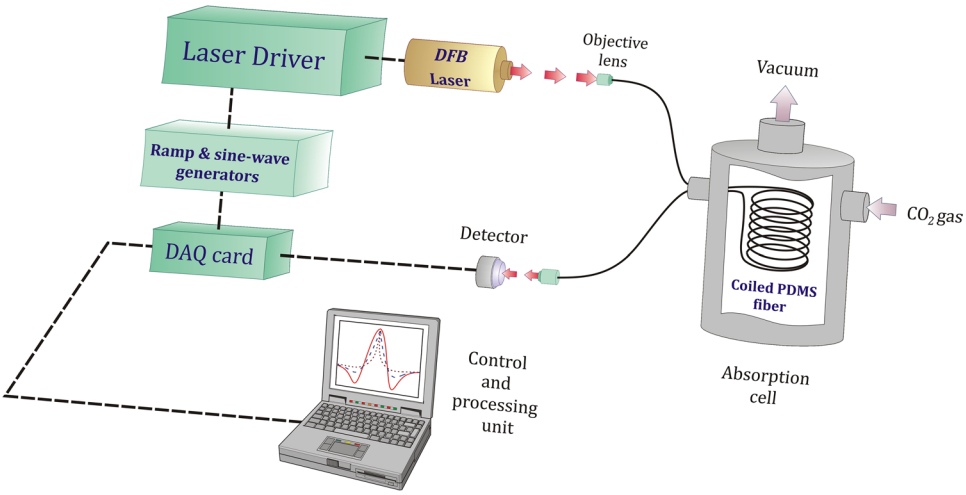

Fig. 7 Experimental arrangement of the PDMS optical fiber-based NIR–DFB laser spectrometer for CO_2 detection using the apodized WMS-2f/1f technique

the intensity of the WMS signal is periodically recorded. Figure 8 illustrates that, after about 3 h, an interaction between the EV field and the diffused CO_2 sample is developed, resulting in the detection of an absorption spectrum that can be distinguished from the noise. In order to verify the sensor performance, reference measurements with a 3-m-long single-pass absorption cell have been performed with about 30 ± 0.1 mbar of CO_2 gas pressure.

As it can be observed, the fabricated sensor shows appreciable sensing characteristics where after about 3 h, the absorption peaks of the CO_2 lines become clearly distinctive from the noise. However, a small drift observed in the plot can be explained by the fact that the two line frequencies acquire different phase velocities in the fiber. To further verify the simulation results presented in the previous section, in Fig. 2, the permeability of the PDMS fiber sensor is experimentally measured and characterized through consecutive tracing of the peak values of the 2f signals. The obtained results are presented in Fig. 9.

As evident from the plot, compared with the calculated results shown in Fig. 2, the same trend can be observed, confirming the useful performance of the fabricated sensor.

The recovery of the sensor is also investigated in the reverse direction by vacuuming the absorption cell and leaving the PDMS fiber inside the cell, while the DFB laser is scanned over the CO_2 lines. We observed that the absorption peaks gradually decayed and finally faded at nearly the same rate and time as specified in Fig. 9. This implies that the CO_2 species were removed from the cladding and therefore the sensor is recovered after an adequate time. This turns out to be very advantageous for guaranteeing that memory of the sensor is relatively erased from the permeated molecules and refreshed for the next and successive measurements in relatively short and repeatable time intervals.

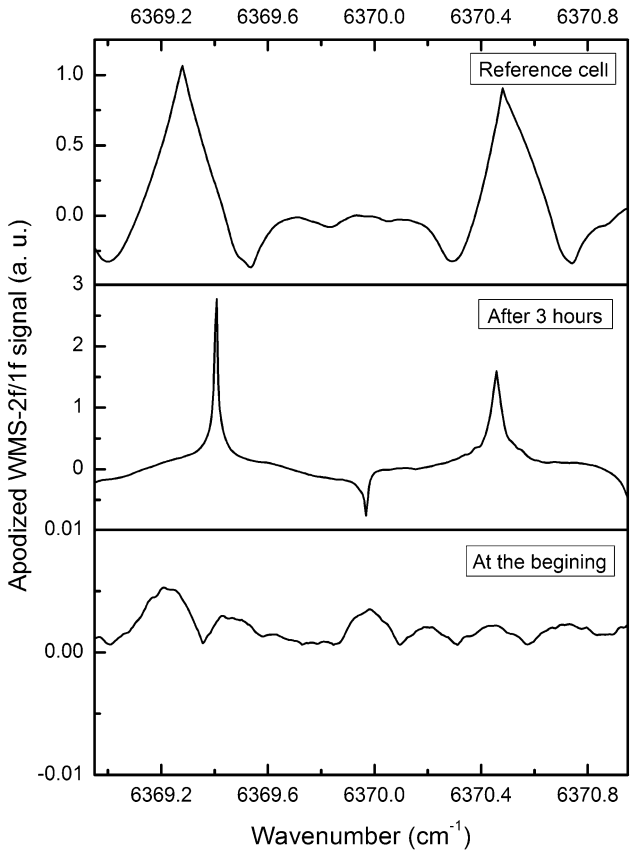

Fig. 8 Periodical monitoring of the apodized WMS-2f/1f signal at the beginning (*bottom*) and after about 3 h (*middle*) of leaving the PDMS fiber sensor inside the high pressure absorption cell, while the DFB laser is simultaneously modulated and scanned over the R(32) and R(34) absorption lines of the CO_2 molecule, respectively, centered at 6,396.408 and 6,370.457 cm^{-1}. Modulation frequency and index and k value are set for 3 kHz, 2.2 and 2, respectively. The reference signal (*top*) is also displayed for the verification of the measurement

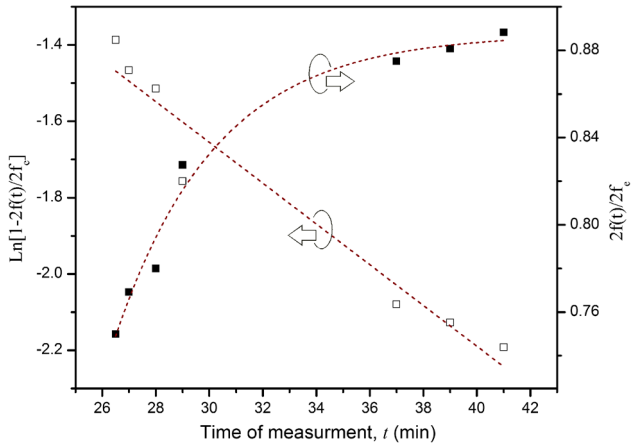

Fig. 9 Permeability characteristics of the PDMS fiber sensor during ~41 min, obtained by experimentally tracing the 2f peak intensities, while the DFB laser is continuously scanned over the R(32) and R(34) absorption lines of the CO_2 molecule, and the stainless absorption cell is kept at 980 ± 10 Torr of gas pressure. The $2f_e$ denotes the steady-state situation at which the 2f peak intensity increases no further

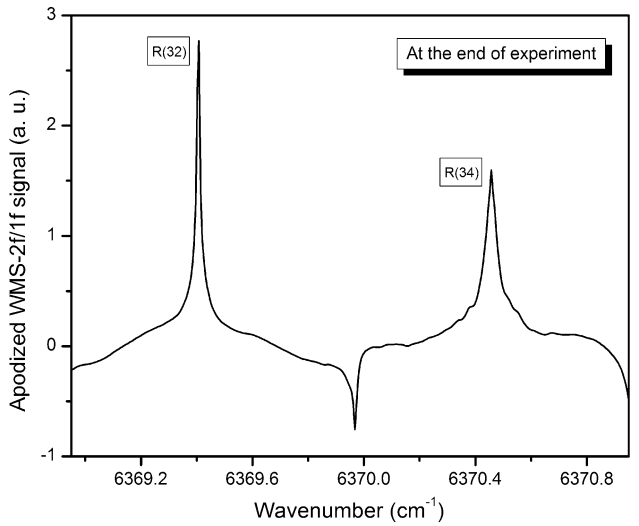

Fig. 10 Experimental trace of the apodized WMS-2f/1f signal after reaching the steady-state condition at which the growth of the absorption peaks of the R(32) and R(34) lines of the CO_2 molecule stops. This takes place after about 4 h from the beginning of the measurement. The modulation index and the frequency are 2.2 and 3 kHz, respectively. The scaling factor is fixed at $k = 2$

The final response of the fabricated sensor is depicted in Fig. 10 where after about 4 h, the apodized signal reaches to the steady-state value, and hence, no noticeable change in the absorption peaks is observed.

Illustrated results in the above plot show high consistency with the simulated and reference signal indicated in Figs. 6 and 8, confirming again the successful performance

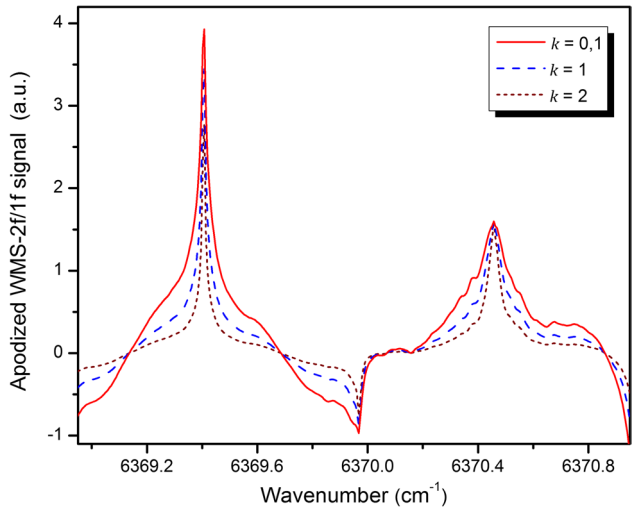

Fig. 11 Trace of the apodized WMS-2f/1f signal for several k values. Experimental circumstances are completely the same as those used in plotting Fig. 10

of the PDMS fiber sensor-based apodized WMS-2f/1f spectrometer. The role of the scaling k factor on the sharpening and narrowing of the signal lineshape is also investigated and represented in Fig. 11.

In confirming the simulation results shown in Fig. 6, it can be seen that greater k values result in sharper and narrower signals, while the peak positions have remained unchanged. As a result, the response feature of the fabricated PDMS fiber sensor shows quite appreciable because, as described by the theory, in this case, the number of modes contributing in the field–matter interaction within the EV area is selectively decreased. This, compared to the case of an uncladded sensor, leads to the weakening of the EV field outside the core. However, experimental results illustrated in Figs. 8, 9, 10 and 11 indicate that the weakening of the EV field is rectified by the unique diffusion and permeability properties of the bent PDMS material which made the sensor very effective and adequate.

4 Conclusion

In this study, we have introduced a CO_2 sensor using a polymer–cladding fiber optic as a sensing element. The permeability characteristics of different polymers are theoretically studied and simulated for a CO_2 gas sample diffusion under a high pressure of 980 Torr. It is found that the PDMS material can be used as a good candidate for the spectroscopy of the CO_2 molecule with appropriate permeability and diffusion coefficients. It was subsequently combined with a so-called apodized WMS-2f/1f method to evaluate and specify the performances of the introduced

sensor in terms of sensitivity and time response. In comparison with the conventional WMS-2f/1f technique, the capability of the apodized WMS-2f/1f method is theoretically investigated for the detection of a CO_2 sample beyond the optically thin limit where very good results are observed without affecting the line properties. Relevant simulation is performed for the R(32) CO_2 absorption line with the specifications inferred from the Hitran database [38]. We have further compared the results of the theoretical simulations using an experimental setup in our laboratory. It is performed by using a coiled and unbuffered PDMS fiber to increase the EV interacting field near the core–cladding interface. By the simultaneous modulation of a NIR–DFB laser with sinusoidal and sawtooth voltages superimposed on the input current of the laser, the apodized WMS-2f/1f tracing of the sample is obtained by scanning the laser's wavelength over the R(32) and R(34) absorption lines of the CO_2 molecule, while the PDMS fiber sensor is kept under 980 $\pm$ 10 Torr of pure CO_2 gas. In addition to the appreciable response time and sensitivity of the fabricated sensor, very good agreement is found between the theoretical simulation and the experimental results. Therefore, the combination of a PDMS fiber sensor and the apodized WMS-2f/1f technique is potentially capable of reaching the adequate level of signal resolution regardless of the limitation of the sample concentration dictated by optical limits. Furthermore, by this method, the narrowing of the signal is significantly enhanced by processing the acquired data with greater scaling factors. Indeed, because the cladding of fiber sensor is not removed, the durability of the fabricated sensor is significantly increased. This makes the sensor as a cost-effective and long lifetime device because it is protected against breakage and environmental perturbations by its polymer cladding. Furthermore, the fabricated sensor is shown reliable and reproducible for successive measurements. This is shown by employing the sensor in the reversed direction when vacuuming the cell, being found that its memory is mostly erased from the permeated CO_2 species at the same trend and rate.

References

1. B.D. Gupta, A. Sharma, C.D. Singh, Fiber optic evanescent field absorption sensor: effect of launching condition and the geometry of the sensing region. Opt. Eng. **33**(6), 1864–1868 (1994)
2. A. Messica, A. Greenstein, A. Katzir, Theory of fiber-optic, evanescent-wave spectroscopy and sensors. Appl. Opt. **35**(13), 2274–2284 (1996)
3. M.S. John et al., A fibre optic evanescent wave sensor for monitoring the rate of pulsed laser deposition of metal thin films. Meas. Sci. Technol. **10**(2), N17 (1999)
4. S.T. Lee et al., Evanescent wave fibre optic sensors for trace analysis of Fe3+ in water. Meas. Sci. Technol. **14**(6), 858 (2003)
5. R. Orghici et al., Fiber optic evanescent field sensor for detection of explosives and CO2 dissolved in water. Appl. Phys. B **90**(2), 355–360 (2008)
6. A. Khorsandi, S. Shojaei, F. Hosseinibalam, Second-harmonic laser-coupled optical fiber sensor for pH measurement and corrosion detection based on evanescent field absorption. Opt. Laser Technol. **44**(5), 1564–1569 (2012)
7. G. Powell et al., In-situ cure monitoring using optical fibre sensors—a comparative study. Smart Mater. Struct. **7**(4), 557 (1998)
8. A. Grazia, M. Riccardo, F.L. Ciaccheri, Evanescent wave absorption spectroscopy by means of bi-tapered multimode optical fibers. Appl. Spectrosc. **52**(4), 546–551 (1998)
9. P. Moar et al., Fabrication, modeling, and direct evanescent field measurement of tapered optical fiber sensors. J. Appl. Phys. **85**(7), 3395–3398 (1999)
10. K. Li, J. Meichsner, In situ infrared fibre evanescent wave spectroscopy as a diagnostic tool for plasma polymerization in a gas discharge. J. Phys. D Appl. Phys. **34**(9), 1318 (2001)
11. M. Kraft et al., Sensor head development for mid-infrared fibre-optic underwater sensors. Meas. Sci. Technol. **13**(8), 1294 (2002)
12. Lu, J., et al. Theoretical analysis of fiber-optic evanescent wave sensors, in *Microwave Conference, 2008 China-Japan Joint*. (IEEE, 2008)
13. A. Millo, Y. Raichlin, A. Katzir, Mid-infrared fiber-optic attenuated total reflection spectroscopy of the solid–liquid phase transition of water. Appl. Spectrosc. **59**(4), 460–466 (2005)
14. Z. Hammody et al., Potential of 'flat'fibre evanescent wave spectroscopy to discriminate between normal and malignant cells in vitro. J. Microsc. **228**(2), 200–210 (2007)
15. S. Yu et al., In vitro glucose measurement using tunable mid-infrared laser spectroscopy combined with fiber-optic sensor. Biomed. Opt. Express **5**(1), 275–286 (2014)
16. F. De-Jun et al., Refractive index sensor based on plastic optical fiber with tapered structure. Appl. Opt. **53**(10), 2007–2011 (2014)
17. Zheng, S., Y. Zhu, and S. Krishnaswamy. Tunable fiber ring laser absorption spectroscopic sensors for gas detection, in *SPIE Smart Structures and Materials + Nondestructive Evaluation and Health Monitoring*. (International Society for Optics and Photonics, 2013)
18. L. Mescia et al., Design of silica-based photonic crystal fiber for biosensing applications. J. Noncryst. Solids **355**(18), 1163–1166 (2009)
19. J. Luo et al., A silver nanoparticle-modified evanescent field optical fiber sensor for methylene blue detection. Sensors **13**(3), 3986–3997 (2013)
20. L. Mescia, F. Prudenzano, Advances on optical fiber sensors. Fibers **2**(1), 1–23 (2013)
21. R. Krska et al., Fiber optic sensor for chlorinated hydrocarbons in water based on infrared fibers and tunable diode lasers. Appl. Phys. Lett. **63**(14), 1868–1870 (1993)
22. P. Hahn et al., Detection of hydrocarbons in water by MIR evanescent-wave spectroscopy with flattened silver halide fibers. Appl. Spectrosc. **55**(1), 39–43 (2001)
23. D.S. Blair, L.W. Burgess, A.M. Brodsky, Study of analyte diffusion into a silicone-clad fiber-optic chemical sensor by evanescent wave spectroscopy. Appl. Spectrosc. **49**(11), 1636–1645 (1995)
24. T. Merkel et al., Gas sorption, diffusion, and permeation in poly (dimethylsiloxane). J. Polym. Sci. Part B Polym. Phys. **38**(3), 415–434 (2000)
25. W. Robb, Thin silicone membranes-their permeation properties and some applications. Ann. N. Y. Acad. Sci. **146**(1), 119–137 (1968)
26. A. D'Orazio et al., Design of planar optic sensors for hydrocarbon detection. Opt. Quant. Electron. **36**(6), 507–526 (2004)

27. F. Prudenzano et al., Design of an optical sensor array for hydrocarbon monitoring. Opt. Quant. Electron. **41**(1), 55–68 (2009)
28. R. St-Gelais et al., Gas sensing using polymer-functionalized deformable Fabry–Perot interferometers. Sens. Actuators B Chem **182**, 45–52 (2013)
29. S.H. Salati, A. Khorsandi, Apodized 2f/1f wavelength modulation spectroscopy method for calibration-free trace detection of carbon monoxide in the near-infrared region: theory and experiment. Appl. Phys. B **116**, 521–531 (2014)
30. B.D. Gupta, B.D. Gupta, *Fiber optic sensors: principles and applications* (New India Publishing Agency, New Delh, 2006)
31. V. Ruddy, B. MacCraith, J. Murphy, Evanescent wave absorption spectroscopy using multimode fibers. J. Appl. Phys. **67**(10), 6070–6074 (1990)
32. A.W. Snyder, J. Love, *Optical waveguide theory* (Springer, Berlin, 1983)
33. A. Ghatak, K. Thyagarajan, *An Introduction to Fiber Optics* (Cambridge University Press, Cambridge, 1998)
34. Y. Xu, A. Cottenden, N.B. Jones, A theoretical evaluation of fibre-optic evanescent wave absorption in spectroscopy and sensors. Opt. Lasers Eng. **44**(2), 93–101 (2006)
35. A. Leung, P.M. Shankar, R. Mutharasan, A review of fiber-optic biosensors. Sens. Actuators B Chem. **125**(2), 688–703 (2007)
36. P. Tremblay et al., Gas permeability, diffusivity and solubility of nitrogen, helium, methane, carbon dioxide and formaldehyde in dense polymeric membranes using a new on-line permeation apparatus. J. Membr. Sci. **282**(1), 245–256 (2006)
37. S. Charati, S. Stern, Diffusion of gases in silicone polymers: molecular dynamics simulations. Macromolecules **31**(16), 5529–5535 (1998)
38. *HITRAN on the web*. 2014